CrossMark

Photocatalysis of cobalt zinc ferrite nanorods under solar light

O. Raina[1] · Rakkiyasamy Manimekalai[1]

Abstract

$Co_{0.7}Zn_{0.3}Fe_2O_4$ nanorods were synthesized from hydrazine precursor by co-precipitation technique. Infrared and thermogravimetric–differential thermogravimetric curves of the precursor indicated the bridging bidentate nature of hydrazine and three-step thermal decomposition. The as-synthesized cobalt zinc ferrite nanorods were characterized by powder X-ray diffraction, scanning electron microscopy, energy dispersive spectroscopy, transmission electron microscopy, vibrating sample magnetometry and UV–diffuse reflection spectroscopy which proposed the phase structure, morphology, magnetic and optical properties. $Co_{0.7}Zn_{0.3}Fe_2O_4$ nanorods showed a sensible photocatalytic activity on Congo red, Malachite green, Methylene blue, Methyl red, Rhodamine B and Rose bengal under solar light at different time intervals and were magnetically separated.

Keywords $Co_{0.7}Zn_{0.3}Fe_2O_4$ · Hydrazine · Bidentate · Nanorods · Photocatalytic

Introduction

Cobalt zinc ferrites have been widely investigated due to their specific electrical [1], optical [2] and magnetic [3, 4] properties. They are gaining attraction because of their applications in microwave absorption [5], sensors [6], magnetic resonance imaging [7] and drug delivery. To date, several methods have been developed to synthesize cobalt zinc ferrites, such as combustion method [8], co-precipitation method [9], microwave combustion method [10], sol–gel auto-combustion method [2], microwave hydrothermal route [11], solution combustion method [12] and modified citrate gel method [13]. Above all, the co-precipitation method is a

✉ Rakkiyasamy Manimekalai
rmanimekalai13@gmail.com

[1] Department of Chemistry, Kongunadu Arts and Science College, Coimbatore, Tamilnadu 641 029, India

versatile approach because it is inexpensive and does not require harsh experimental conditions.

Nowadays, the presence of organic dyes in water bodies is cited as one of the critical global problems due to industrialization [14–16]. Because of that, much attention has been paid by researchers to develop various novel technologies for water purification [17, 18]. Among those, photocatalytic degradation of synthetic dyes using nanocatalyst is an effective technique [19]. Meanwhile, ferrites are also effective in the degradation of many potential organic contaminants [20–26]. Hitherto, the photodegradation of organic dyes using cobalt zinc ferrite nanoparticles have been scarcely reported [20, 27].

Since utilization of solar energy is an ideal pathway for this purpose [28, 29], our present study is focused on the photocatalysis of cobalt zinc ferrite nanoparticles under solar light synthesized from the hydrazinated precursor [30] by co-precipitation technique. The photocatalytic activity of as-said nanoparticle is analyzed for the degradation of Congo red (CR), Malachite green (MG), Methylene blue (MB), Methyl red (MR), Rhodamine B (RhB) and Rose bengal (RB) in aqueous solution at different time intervals under bright solar light.

Experimental

Materials

All of the chemical reagents were purchased from Merck, India, in analytical reagent (AR) grade and used without further purification. Distilled water was used for all of the solutions. The following reagents were used: 2,4-dichlorophenoxy-acetic acid, hydrazine hydrate (99%), iron sulfate heptahydrate, cobalt nitrate hexahydrate, zinc nitrate hexahydrate, ethanol, diethylether, concentrated hydrochloric acid, carbontetrachloride, CR, MG, MB, MR, RhB and RB.

Synthesis of $Co_{0.7}Zn_{0.3}Fe_2O_4$ nanorods

$Co_{0.7}Zn_{0.3}Fe_2O_4$ nanorods were prepared from the inorganic precursor through co-precipitation technique by the addition of an aqueous solution (50 ml) of hydrazine hydrate (0.0199 mol) and 2,4-dichlorophenoxyacetic acid (0.01 mol) to the corresponding aqueous solution (50 ml) containing ferrous sulphate heptahydrate (0.01 mol), cobalt nitrate hexahydrate (0.0061 mol) and zinc nitrate hexahydrate (0.0012 mol). The mixed solutions were stirred magnetically for half an hour. The formed yellow precipitate was filtered and washed with water, alcohol, diethylether and air-dried. This precursor was thermally decomposed in air for 1 hour which led to the formation of $Co_{0.7}Zn_{0.3}Fe_2O_4$ nanorods.

Characterization

Infrared (IR) spectra were recorded by the KBr disk technique using a Shimadzu spectrophotometer. Simultaneous thermogravimetry–differential thermogravimetry

analysis (TG–DTA) was carried out in air using a Universal V4.5A instrument. Scanning electron microscopy (SEM) and energy dispersive spectroscopy (EDS) images were performed on a HITACHI Model S-3000H. X-ray diffraction (XRD) patterns were recorded using an X-ray diffractometer (X'pert PRO model) using Cu-Ka radiation, at 40 keV in the 2-h range of 20–90°. Transmission electron microscopy (TEM) micrographs were collected on a Joel/JEM 2100 instrument. The UV–diffuse reflectance spectrum (UV–DRS) was operated on a Shimadzu UV–DRS spectrophotometer. The room-temperature magnetic parameter measurement was performed using a Lakeshore VSM 7410 magnetometer. The adsorption and photocatalytic activity studies were carried out on a Shimadzu UV-2550 UV–Vis spectrophotometer.

Photocatalytic test

The photocatalytic activity of $Co_{0.7}Zn_{0.3}Fe_2O_4$ nanorods was evaluated by the degradation of CR, MG, MB, MR, RhB and RB under bright solar light. The $Co_{0.7}Zn_{0.3}Fe_2O_4$ nanorods as a catalyst (200 mg) were added to a flask containing 100 ml of dye solutions with an initial concentration of 500 mg l^{-1} under magnetic stirring for 1 hour in the dark to attain adsorption–desorption equilibrium. After that, the suspensions were kept under solar light and the samples were collected at different time intervals (0, 10, 20, 30, 40, 50 and 60 min). The concentrations of dyes were determined at wavelengths of 496, 664, 615, 532, 550 and 554 nm for CR, MB, MG, MR, RB and RhB, respectively.

Results and discussion

Characterization of the precursor

The hydrazine content (5.7%) in the precursor was determined by titration using KIO_3 as titrant, by volumetric analysis under Andrew's condition [31]. The percentages of cobalt (0.78%), zinc (0.34%) and iron (2.52%) in the precursor were confirmed by EDS analysis (Fig. 1). From these data, the molecular stoichiometric composition of the precursor was assigned as $Co_{0.7}Zn_{0.3}Fe_2(C_6H_3Cl_2OCH_2COO)_4 \cdot 2N_2H_4$ and confirmed by thermal analysis.

Figure 2 shows the infrared spectrum of the precursor. Three bands in the region 3255–3340 cm^{-1} are due to the N–H stretching frequency. The N–N stretching frequency observed at 948 cm^{-1} confirmed the bidentate bridging nature of hydrazine [32]. The separation of asymmetric and symmetric stretching frequency of carboxylate found at 240 cm^{-1}, which documented monodentate linkage [32] of the carboxylate group. The band at 454 cm^{-1} indicated the presence of a metal/oxygen bond [33].

TG–DTA curves of the precursor showed four steps of mass loss and endothermic peaks (Fig. 3). A very small endothermic peak was observed as the initial step. The mass loss of 5.74% corresponds to the elimination of two hydrazine molecules with increase from room temperature to 180 °C. The strong endotherm
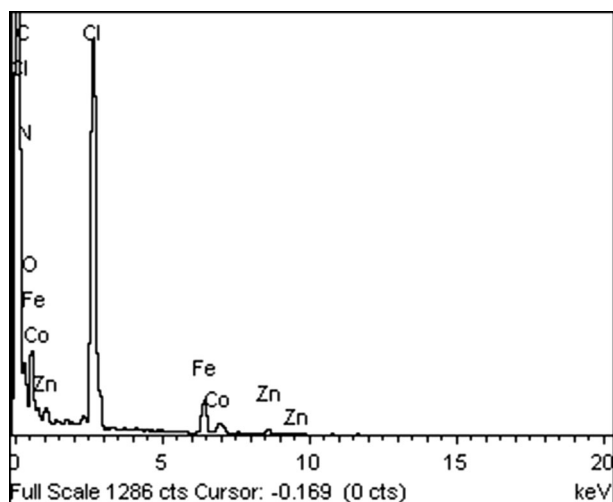
Fig. 1 EDS spectra of $Co_{0.7}Zn_{0.3}Fe_2(C_6H_3Cl_2OCH_2COO)_4 \cdot 2N_2H_4$
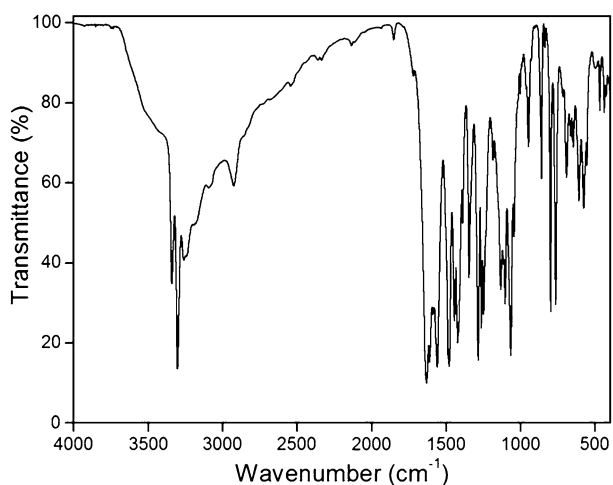
Fig. 2 IR spectra of $Co_{0.7}Zn_{0.3}Fe_2(C_6H_3Cl_2OCH_2COO)_4 \cdot 2N_2H_4$

observed in the region 180–310 °C is due to the beginning of decarboxylation with a 39.4% mass loss. In the region 310–580 °C, complete decarboxylation takes place. Thus, the precursor $Co_{0.7}Zn_{0.3}Fe_2(C_6H_3Cl_2OCH_2COO)_4 \cdot 2N_2H_4$ was thermally decomposed in air to yield $Co_{0.7}Zn_{0.3}Fe_2O_4$ nanorods [34].

Characterization of $Co_{0.7}Zn_{0.3}Fe_2O_4$ nanorods

Figure 4 shows XRD pattern of $Co_{0.7}Zn_{0.3}Fe_2O_4$ nanorods. The characteristic peaks coincide exactly with the JCPDS card nos. 73-1963 ($ZnFe_2O_4$) and 22-1086

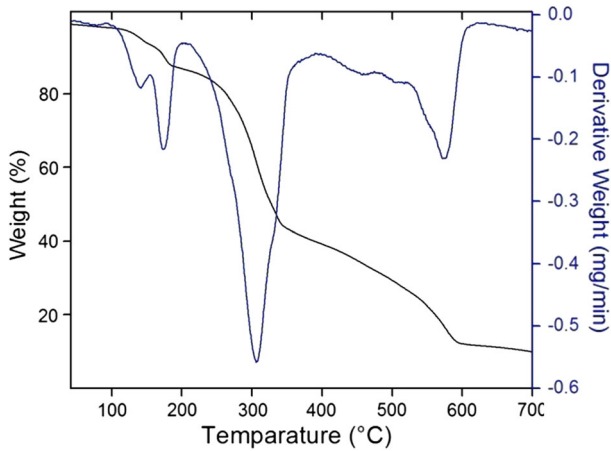**Fig. 3** TG-DTA curve of $Co_{0.7}Zn_{0.3}Fe_2(C_6H_3Cl_2OCH_2COO)_4 \cdot 2N_2H_4$

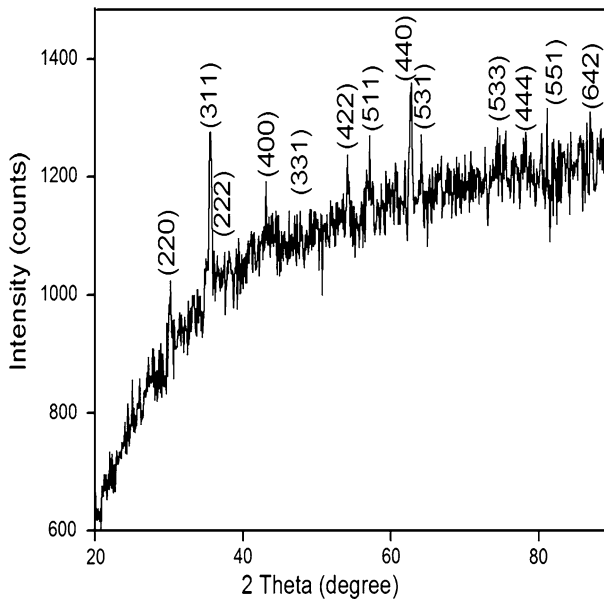**Fig. 4** XRD spectra of $Co_{0.7}Zn_{0.3}Fe_2O_4$ nanorods

$(CoFe_2O_4)$. The sharp and intense XRD peaks revealed their nanocrystalline nature [35] as confirmed by the selected area electron diffraction (SAED) pattern (Fig. 6d). The average crystallite size of the nanorods calculated from Scherrer's formula is 14 nm.

The IR spectrum of $Co_{0.7}Zn_{0.3}Fe_2O_4$ nanorods (Fig. 5) showed the characteristic peaks of tetrahedral and octahedral Fe–O stretching bands at 530 and 420 cm^{-1}, respectively. The other characteristic bands of N–N and N–H stretching frequencies
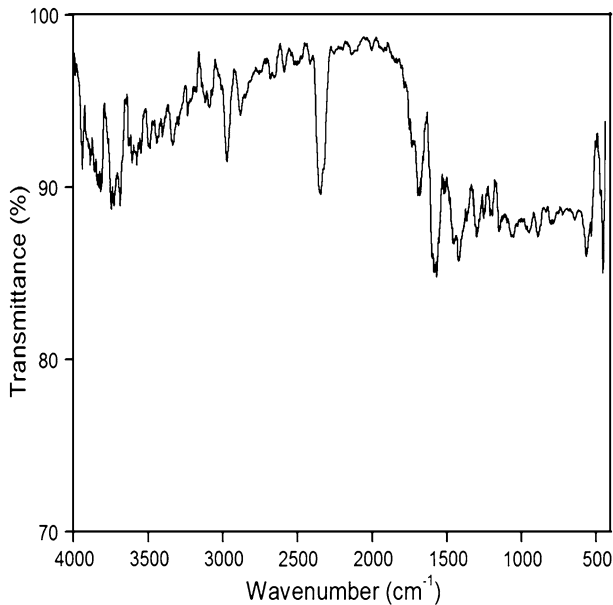
Fig. 5 IR spectra of $Co_{0.7}Zn_{0.3}Fe_2O_4$ nanorods

observed in the precursor (Fig. 2) had vanished. Thus, the formation of $Co_{0.7}Zn_{0.3}$-Fe_2O_4 nanorods from the precursor was further confirmed.

Figure 6a presents an SEM image of $Co_{0.7}Zn_{0.3}Fe_2O_4$ nanorods. As seen in the image, agglomeration in the particles exhibits irregular nanorod-like morphology interconnected with each other. EDS spectra (Fig. 6b) confirmed that the nanorods are mainly composed of Co, Zn, Fe and O. Figure 6c shows a TEM image of the nanorods, indicating a particle size of around 20 nm, which closely matched the size calculated by Scherrer's equation. The SAED pattern (Fig. 6d) exhibits spots forming rings corresponding to (311), (400), (331), (440), (444) and (642) planes indicated polycrystalline nature of the sample.

Figure 7 illustrates the room-temperature magnetic parameter measurement of $Co_{0.7}Zn_{0.3}Fe_2O_4$ nanorods. A saturation magnetization (M_s) of 14.5 emu g^{-1}, remanent magnetization (M_r) of 2.2 emu g^{-1} and a coercivity (H_c) of 306.41 Oe were observed. The hysteresis loop reveals that the soft magnetic nature and excellent magnetic properties were maintained to some extent.

The UV–DRS of $Co_{0.7}Zn_{0.3}Fe_2O_4$ nanorods (Fig. 8) exhibits strong absorption between 200 and 800 nm and an absorption edge at 418 nm. The optical band gap (E_g) can be calculated as 2.9 eV. The low band gap energy and particle size were the driving forces for acceptable photocatalytic activity of the nanorods under solar light.
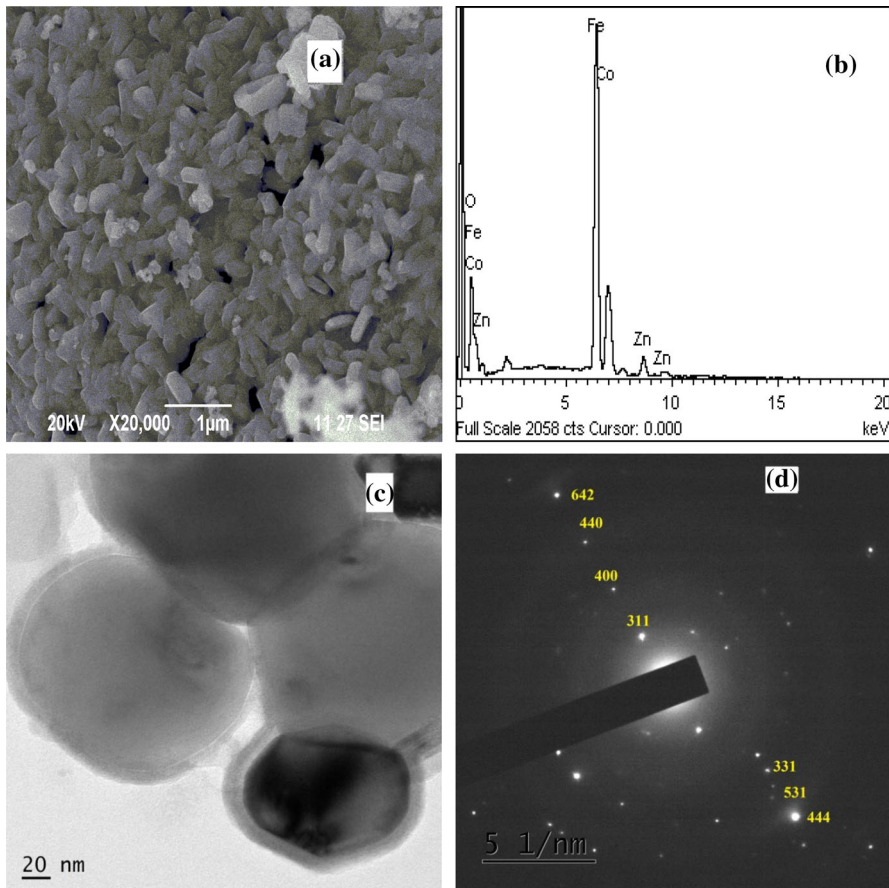
Fig. 6 SEM image (**a**), EDS spectrum (**b**), TEM image (**c**) and SAED pattern (**d**) of $Co_{0.7}Zn_{0.3}Fe_2O_4$ nanorods

Photocatalytic properties and adsorption kinetics

The photodegradation of dyes (CR, MB, MG, MR, RB and RhB) under bright solar light using $Co_{0.7}Zn_{0.3}Fe_2O_4$ nanorod as a catalyst was evaluated. In the photocatalytic test, the reaction time differs with respect to dyes: 50 min (CR and MB), 40 min (MG, RhB and RB) and 30 min (MR). The photocatalytic degradation of dyes was shown to follow the order: CR > RB > MB > MR > RhB > MG (Fig. 9a). It can be clearly seen that 58% of CR and RB molecules in the solution degraded after 40 min. The catalyst was separated by an external magnet for recycling (Fig. 9b).

Figure 9c reveals the relationship between the time and the equilibrium adsorption (q_e) of various dyes on $Co_{0.7}Zn_{0.3}Fe_2O_4$ photocatalyst. Equation (1) is used to calculate the equilibrium uptake:

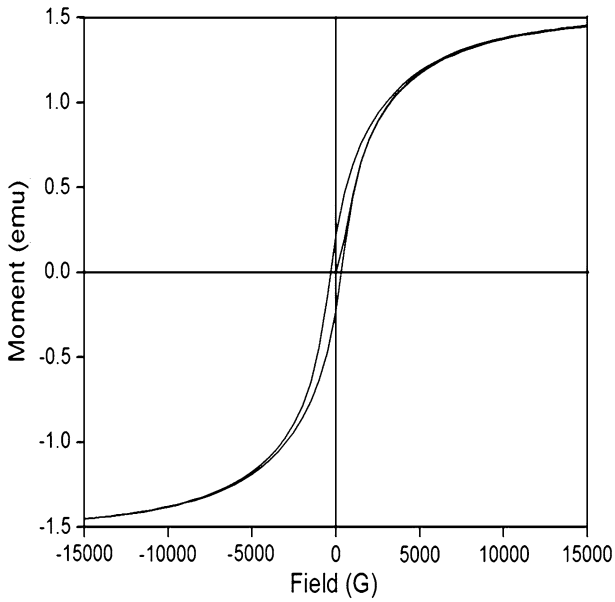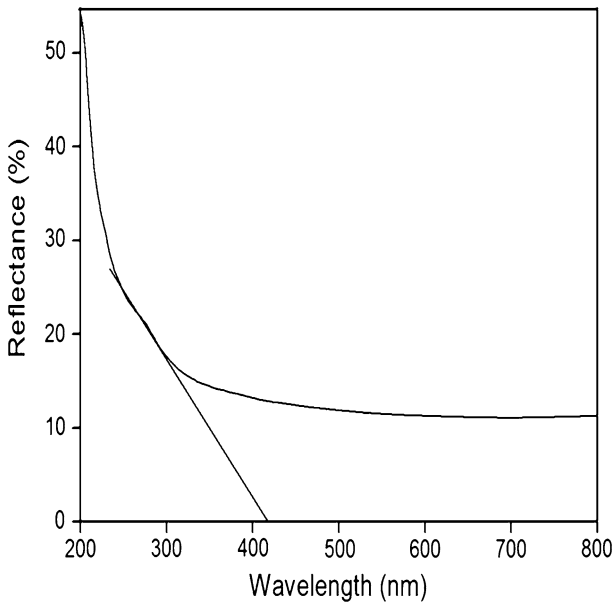**Fig. 7** VSM hysteresis loop of $Co_{0.7}Zn_{0.3}Fe_2O_4$ nanorods

Fig. 8 UV–DRS spectrum of $Co_{0.7}Zn_{0.3}Fe_2O_4$ nanorods

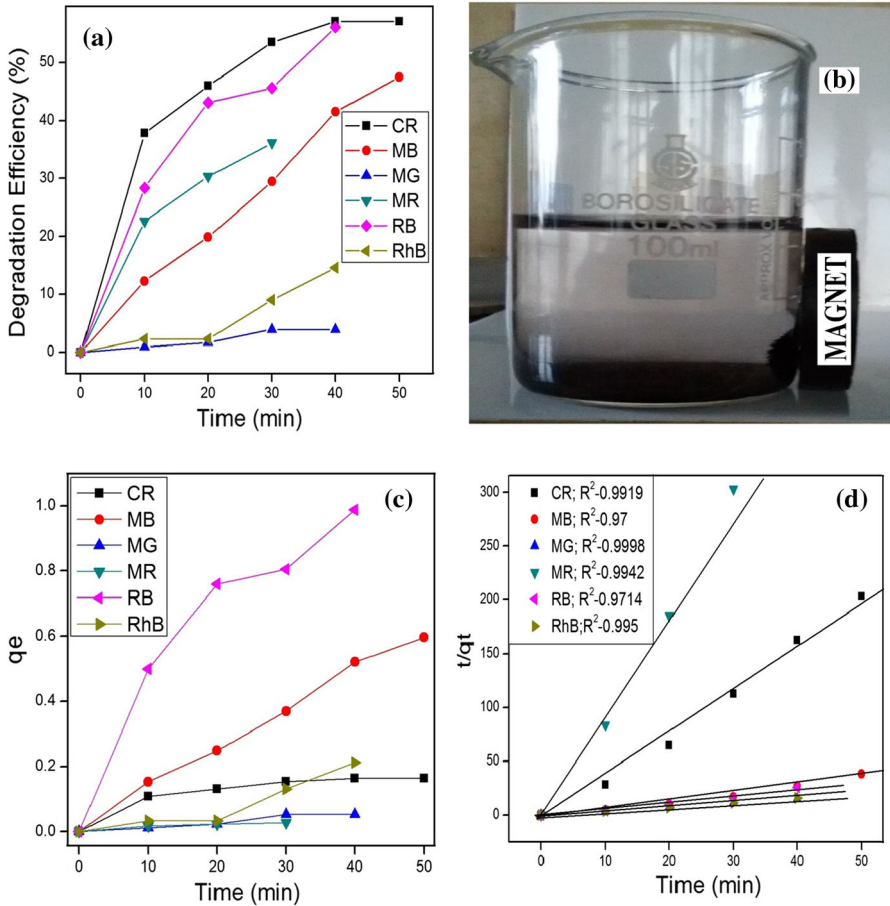**Fig. 9 a** Degradation efficiency of dyes. **b** Magnetic separation property of $Co_{0.7}Zn_{0.3}Fe_2O_4$ photocatalyst. **c** Adsorption capacity of dyes with time and **d** pseudo-second-order kinetic plots for the removal of dyes on $Co_{0.7}Zn_{0.3}Fe_2O_4$ photocatalyst under solar light

$$q_{\mathrm{e}} = \frac{(C_0 - C_{\mathrm{e}})V}{W} \tag{1}$$

where q_{e} is the amount of dye adsorbed by catalyst at equilibrium, C_0 is the initial concentration of the dye solution in mg l^{-1}, C_{e} is the equilibrium concentration of the dye solution in mg l^{-1}, V is the volume of the solution in ml and W is the mass of catalyst in milligrams taken for the experiments. It is obvious that there was significant adsorption of RB and MB, while there was a moderate adsorption of RhB, CR, MG and MR.

Equation (2) represents the adsorption kinetics as explained by a second-order model:

$$\frac{t}{q_t} = \frac{1}{k_2 q_e 2} + \frac{t}{q_e} \tag{2}$$

where k_2 is the rate constant for second-order adsorption (g mg^{-1} min^{-1}), and q_e and k_2 were determined from the slope and intercept of plot t/qt versus t (Fig. 9d) for various dyes. The linear plot with correlation coefficient R^2 concluded that the pseudo-second-order adsorption model was suitable for fitting the adsorption kinetics.

Conclusion

A $Co_{0.7}Zn_{0.3}Fe_2O_4$ photocatalyst was synthesized by thermal decomposition technique from its precursor $Co_{0.7}Zn_{0.3}Fe_2(C_6H_3Cl_2OCH_2COO)_2 \cdot 2N_2H_4$. The chemical formula was fixed by the data observed from EDS, IR and TG–DTA of the precursor. The TG–DTA showed three-step decomposition which led to the formation of $Co_{0.7}Zn_{0.3}Fe_2O_4$ photocatalyst. The sharp and intense XRD peaks suggested a polycrystalline nature and the crystallite size calculated as 14 nm from the Debye–Scherrer formula was confirmed by TEM. Nanorods with agglomeration were observed in the SEM image while EDS showed the presence of the expected elements. The soft magnetic nature of the photocatalyst was observed from the VSM hysteresis loop. From the photodegradation of CR, MB, MG, MR, RB and RhB, it can be concluded that $Co_{0.7}Zn_{0.3}Fe_2O_4$ nanorods are an efficient magnetic photocatalyst and magnetically separable for the recycling process.

Compliance with ethical standards

Conflict of interest The authors declare that they have no conflict of interest.

References

1. D.K. Pradhan, S. Kumari, V.S. Puli, P.T. Das, D.K. Pradhan, A. Kumar, J.F. Scott, R.S. Katiyar, Phys. Chem. Chem. Phys. **19**, 210 (2016)
2. I.M. Abdulmajeed, L.S. Khalil, Int. J. Curr. Eng. Technol. **6**, 976 (2016)
3. F.S.M. Doulabi, M. Mohsen-Nia, Iran. Polym. J. **22**, 9 (2013)
4. T. Tatarchuk, M. Bououdina, W. Macyk, O. Shyichuk, N. Paliychuk, I. Yaremiy, B. Al-Najar, M. Pacia, Nanoscale Res. Lett. **12**, 141 (2017)
5. X. Huang, J. Zhang, W. Rao, T. Sang, B. Song, C. Wong, J. Alloys Compd. **662**, 409 (2016)
6. N. Somaiah, T.V. Jayaraman, P.A. Joy, D. Das, J. Magn. Magn. Mater. **324**, 2286 (2012)
7. Z. Ghasemian, D. Shahbazi-Gahrouei, S. Manouchehri, Avicenna J. Med. Biotechnol. **7**, 64 (2015)
8. M.H. Yousefi, S. Manouchehri, A. Arab, M. Mozaffari, R. Amiri, J. Amighian, Mater. Res. Bull. **45**, 1792 (2010)
9. P. Yaseneva, M. Bowker, G. Hutchings, Phys. Chem. Chem. Phys. **13**, 18609 (2011)
10. M. Sundararajan, L.J. Kennedy, J.J. Vijaya, J. Nanosci. Nanotechnol. **15**, 6719 (2015)
11. K. Praveena, K. Sadhana, Int. J. Sci. Res. Pub. **5**, 1 (2015)
12. R. Rani, S.K. Sharma, K.R. Pirota, M. Knobel, S. Thakur, M. Singh, Ceram. Int. **38**, 2389 (2012)

13. E. Girgis, M.M.S. Wahsh, A.G.M. Othman, L. Bandhu, K.V. Rao, Nanoscale Res. Lett. **6**, 1 (2011)
14. R. Kant, Nat. Sci. **4**, 22 (2012)
15. M. Balakrishnan, S.A. Antony, S. Gunasekaran, R.K. Natarajan, Indian J. Sci. Technol. **1**, 1 (2008)
16. Z. Carmen, S. Daniela, Organic pollutants ten years after the Stockholm convention—environmental and analytical update, ed. By T. Puzyn (In Tech, 2012), p. 55
17. X. Qu, P.J.J. Alvarez, Q. Li, Water Res. **47**, 3931 (2013)
18. A. Ahmad, S.H. Mohd-Setapar, S.C. Chuo, A. Khatoon, W.A. Wani, R. Kumar, M. Rafatulla, RSC Adv. **5**, 30801 (2015)
19. E. Casbeer, V.K. Sharma, X.-Z. Li, Sep. Purif. Technol. **87**, 1 (2012)
20. G. Fan, J. Tong, F. Li, Ind. Eng. Chem. Res. **51**, 13639 (2012)
21. K. Zaharieva, V. Rives, M. Tsvetkov, Z. Cherkezova-Zheleva, B. Kunev, R. Trujillano, I. Mitov, M. Milanova, Mater. Chem. Phys. **160**, 271 (2015)
22. S.D. Jadhav, P.P. Hankare, R.P. Patil, R. Sasikala, Mater. Lett. **65**, 371 (2011)
23. P. Guo, M. Lv, G. Han, C. Wen, Q. Wang, H. Li, X.S. Zhao, Materials **9**, 806 (2016)
24. P.P. Hankare, R.P. Patil, A.V. Jadhav, K.M. Garadkar, R. Sasikala, Appl. Catal. B **107**, 333 (2011)
25. L. Han, X. Zhou, L. Wan, Y. Deng, S. Zhan, J. Environ. Chem. Eng. **2**, 123 (2014)
26. K.N. Harish, H.S.B. Naik, P.N.P. Kumar, R. Viswanath, ACS Sustain. Chem. Eng. **1**, 1143 (2013)
27. C. Lin, X. Xie, C. Li, Q. Yan, Mater. Sci. Semicond. Process. **82**, 46 (2018)
28. Z. Zhang, X. Jiang, B. Liu, L. Guo, N. Lu, L. Wang, J. Huang, K. Liu, B. Dong, Adv. Mater. **30**, 1705221 (2018)
29. Z. Zhang, J. Huang, Y. Fang, M. Zhang, K. Liu, B. Dong, Adv. Mater. **29**, 1606688 (2017)
30. S. Rangasamy, K. Kalimuthu, M. Rakkiasamy, Synth. React. Inorg. Metal-Org. Nano-Metal Chem. **45**, 482 (2015)
31. A.I. Vogel, *Vogel's Text book of Quantitative Chemical Analysis*, 5th edn. (Longmann, London, 1989), p. 384
32. A. Braibanti, F. Dallavalle, M.A. Pellinghelli, E. Leporati, Inorg. Chem. **7**, 1430 (1968)
33. M.G. Naseri, E.B. Saion, M. Hashim, A.H. Shaari, H.A. Ahangar, Solid State Commun. **151**, 1031 (2011)
34. U.B. Gawas, V.M.S. Verenkar, Thermochim. Acta **556**, 41 (2013)
35. R.C.C. Monteiro, A.A.S. Lopes, M.M.R.A. Lima, J.P.B. Veiga, J. Non-Cryst. Solids **491**, 124 (2018)